Bioactive Materials 6 (2021) 4816–4829

Contents lists available at ScienceDirect

Bioactive Materials

journal homepage: www.sciencedirect.com/journal/bioactive-materials

An injectable and self-healing hydrogel with controlled release of curcumin to repair spinal cord injury

Jinghua Luo [a,c,1], Xueshuang Shi [a,1], Liming Li [a], Zan Tan [b], Feng Feng [b], Jun Li [a], Mao Pang [b], Xiaoying Wang [c], Liumin He [a,b,c,*]

[a] MOE Joint International Research Laboratory of CNS Regeneration, Jinan University, Guangzhou, 510632, China
[b] Department of Spine Surgery, The 3rd Affiliated Hospital, Sun Yat-Sen University, Guangzhou, 510630, China
[c] College of Life Science and Technology, Jinan University, Guangzhou, 510630, China

ARTICLE INFO

Keywords:
Spinal cord injury
Injectable and self-healing hydrogel
Curcumin
Schwann cells

ABSTRACT

The harsh local micro-environment following spinal cord injury (SCI) remains a great challenge for neural regeneration. Local reconstitution of a favorable micro-environment by biocompatible scaffolds with desirable functions has thus been an area of concern. Herein, a hybrid hydrogel was developed using Fmoc-grafted chitosan (FC) and Fmoc peptide (FI). Dynamic reversible π-π stacking interactions of the fluorenyl rings enabled the FC/FI hybrid hydrogel to exhibit excellent injectable and self-healing properties, as characterized by visual appearances and rheological tests. Furthermore, the FC/FI hybrid hydrogel showed a slow and persistent release of curcumin (Cur), which was named as FC/FI-Cur hydrogel. *In vitro* studies confirmed that with the support of FC/FI-Cur hydrogel, neurite outgrowth was promoted, and Schwann cell (SC) migration away from dorsal root ganglia (DRG) spheres with enhanced myelination was substantiated. The FC/FI-Cur hydrogel well reassembled extracellular matrix at the lesion site of rat spinal cord and exerted outstanding effects in modulating local inflammatory reaction by regulating the phenotypes of infiltrated inflammatory cells. In addition, endogenous SCs were recruited in the FC/FI-Cur graft and participated in the remyelination process of the regenerated nerves. These outcomes favored functional recovery, as evidenced by improved hind limbs movement and enhanced electrophysiological properties. Thus, our study not only advanced the development of multifunctional hydrogels but also provided insights into comprehensive approaches for SCI repair.

1. Introduction

Traumatic spinal cord injury (SCI) inevitably triggers an acute inflammation followed by multiple pathology events such as extensive cell death, axonal demyelination, and the development of glial fibrosis sealing a fluid-filled cystic cavity, which together makes SCI therapy extremely difficult [1,2]. Over the past decades, abundant efforts have been devoted to develop curative treatments for neural regeneration. Cell-based regenerative medicine strategy is a reasonable and promising therapy for SCI by supplementing new neural cells [3] as well as regulating inflammatory reactions [4], however poor survival of transplanted cells in the harsh environment makes it challenging. Local administration of neuroprotective factors and anti-inflammatory drugs has been employed with the aim of reversing the growth-inhibiting environment of axons [5]. These therapies, however, still suffer from limited efficiency due to rapid elimination by cerebrospinal fluid and impaired bioactivity. Therefore, direct delivery of cells and/or bioactive molecules is often less effective in SCI repair and may lead to the failure of neural regeneration [3].

Remyelination plays an important role in axon regeneration and functional recovery. In the nervous system, myelin facilitates rapid signal conduction in axons. Functional impairment would be aggravated following SCI as demyelination of spared axons slows conduction or causes complete conduction block across the lesion site [6]. Moreover, demyelination due to prolonged and widespread oligodendrocyte apoptosis causes a lack of trophic support from myelin-forming cells, which makes spared axons vulnerable to damage. Endogenous oligodendrogenesis and remyelination processes show advantages over

Peer review under responsibility of KeAi Communications Co., Ltd.
* Corresponding author. MOE Joint International Research Laboratory of CNS Regeneration, Jinan University, Guangzhou, 510632, China.
E-mail address: helm9@mail.sysu.edu.cn (L. He).
[1] Jinghua Luo and Xueshuang Shi contributed equally to this work.

https://doi.org/10.1016/j.bioactmat.2021.05.022
Received 21 March 2021; Received in revised form 8 May 2021; Accepted 8 May 2021

transplantation of myelinating cells regarding sources, immunologic rejection, and ethical issues. However, it is still limited by excitotoxicity and the upregulation of remyelination-inhibitory molecules in the post-injury microenvironment. Moreover, oligodendrocyte precursor cells, the myelinating cells native to the central nervous system, would alter gene expression following demyelination [6]. Schwann cells (SCs) are alternative candidates, which are widely used to activate endogenous myelination after SCI. Dorsal root entry zone would be damaged following SCI, and SCs would migrate into the lesion site from the nerve roots, myelinating the regenerated or demyelinated axons in the injured spinal cord and then restoring conduction activity [7,8]. However, due to lack of structural support, only a small number of SCs being able to accumulate in the lesion site of the spinal cord limits the contribution of endogenous remyelination by SCs [9].

Modulation of the post-injury microenvironment is of great importance in repairing SCI. Employment of biomaterials emerges as a promising strategy by providing a structural substrate for endogenous cells and regenerating axons [10]. Given that the spinal cord is a highly hydrated soft "material", hydrogels with physicochemical and mechanical properties similar to natural extracellular matrix showing significant advantages over stiff scaffolds, e.g. the risk of tissue damage due to mechanical mismatch could be well avoided [11–14]. They could be further tailored to be injectable, which would completely fill the cavity in a noninvasive manner, regardless of the size and shape [15]. To prolong the lifespan of the hydrogel, self-healing concept has been explored. A self-healing hydrogel could realize self-repair for mechanical damage as well as maintain an integrated structure over neural regeneration. Such a property is highly favorable for long-term *in vivo* application as complex physiological environment and stress induced by body movement impair the mechanical durability of the hydrogel, and weaken their chronic performances [16–18]. The self-healing behavior is mainly based on the reversible covalent bonds and/or noncovalent interactions of the hydrogel molecules, which acquire rapid equilibrium between the reversible dissociation and recombination of components [12]. Structural integrity and persistent functions in long-term transplantation are thus ensured simultaneously.

In the current study, an injectable hydrogel with self-healing property was fabricated from chitosan grafted with N-terminus with fluorenylmethoxycarbonyl (Fmoc) group, defined as FC, and a Fmoc peptide. Chitosan is a natural macromolecule favorable for neural cells and widely used for neural regeneration. The laminin-derived peptide IKVAV (Ile-Lys-Val-Ala-Val) that promotes neurite outgrowth was conjugated to Fmoc group, defining as FI. Abundant π-π stacking interactions of the fluorenyl rings in the Fmoc moieties, which are expected to serve as physically cross-linked points in FC/FI hybrid hydrogel, are reversible, endowing the hybrid hydrogel with good injectability and self-healability. The hybrid hydrogel could well reassemble extracellular matrix locally at the lesion site for regenerating axons and endogenous cells. Furthermore, curcumin (Cur) was encapsulated in the hybrid hydrogel and would be released in a sustained pattern. As a polyphenol extract derived from plants of the genus Curcuma, Cur has been well known for its anti-oxidant and anti-inflammatory pharmacological activities [19]. Besides, studies have demonstrated that Cur showed neuroprotective effects by inhibiting neuronal apoptosis and improved remyelination, contributing to functional neurologic recovery after SCI [20,21]. Liu et al. and Zhao et al. found that Cur promoted the upregulation of S100 expression in SCs, and thus improved myelin structure and functional recovery of the sciatic nerve [22,23]. However, to the best of our knowledge, there are few reports on the therapeutic role of Cur in SCI with respect to SC-related remyelination.

Considerable evidence indicates that SCI repair would not be achievable with a single therapeutic strategy and multiple interventions have been consensus. In our study, the roles of the multifunctional hydrogel system were thoroughly investigated in promoting neural regeneration after SCI. Taken together, this study sheds light on the advancement of biomaterial-based strategy in repairing SCI.

2. Materials and methods

2.1. Material

Chitosan (CS) (MW 100,000 Da, 80% deacetylation) was purchased from Meilun Biological Technology Co., Ltd (Dalian, China). Fmoc-glycine (Fmoc-G) and curcumin (98% purity) was purchased from J&K Scientific Ltd (Shanghai, China). 1-ethyl-3-(3-dimethyl-aminopropyl) carbodiimide hydrochloride (EDC) and N-hydroxysuccinimide (NHS) were purchased from Meryer Chemical Technology Co., Ltd. (Shanghai, China). Dimethyl sulfoxide (DMSO) was supplied from Beyotime Biotechnology Company (Shanghai, China). Dialysis membranes with a molecular weight cur-off (MWCO) of 3000 Da were supplied from Shanghai Yuanye Bio-Technology Co., Ltd (Shanghai, China). The designer peptide Fmoc-RRIKVAV (FI) was custom-synthesized by BACHEM AG. All other chemicals were of analytical grade and used as received without further purification.

2.2. Synthesis of fluorenyl functionalized chitosan (FC)

Chitosan modified with fluorenyl groups (FC) was performed by standard EDC/NHS coupling chemistry. Briefly, 677 mg CS (4 mmol, 1 euqiv.) was dissolved in 100 mL 0.1 M hydrochloric acid (HCl) under stirring at 25 °C. Meanwhile, 2.378 g Fmoc-G (8 mmol, 2euqiv.) were dissolved in 40 mL dimethyl sulfoxide under stirring for 30 min at 25 °C. 4.60 g EDC (24 mmol, 6 euqiv.) and 2.762 g NHS (24 mmol, 6 euqiv.) were dissolved in 10 mL dimethyl sulfoxide. Next, the EDC/NHS solution was added to the Fmoc-G solution under stirring for 30 min. Subsequently, the Fmoc-G solution was added dropwise slowly to the CS solution. The pH value of the reaction mixture was adjusted to 5.5–6.0 by the addition of 1 M NaOH and reacted at 25 °C for 24 h under constant stirring. After the reaction, the solution was dialyzed using a dialysis membrane (3000 MWCO) for 3 days against deionized water, while the dialysis solvent was replaced with fresh one every 8 h. The final sample was finally lyophilized to get FC powders.

2.3. Preparation of hydrogels

Peptide Fmoc-RRIKVAV (FI) was dissolved in deionized water under stirring at 25 °C to form 1% (w/v) solution and get the homogeneous solution. Once dissolved, an appropriate amount of FC was added to the FI solution to reach a final concentration of 10% (w/v). Next, the pH of the solution mixture was adjusted to 7.4 by the addition of 1 M Tris-HCl. The final hydrogel was named FC/FI hydrogel.

Hydrogels without FI were prepared in an analogous way. Briefly, FC was dissolved in deionized water under stirring at 25 °C to reach a final concentration of 10% (w/v) and get the homogeneous hydrogel. The final hydrogel was named FC hydrogel.

Curcumin-loaded FC (FC-Cur) hydrogel was prepared to evaluate the release kinetics in vitro. Briefly, curcumin was dissolved in DMSO at 10 mM under stirring until completely dissolved. Next, curcumin solution was diluted to 100 μM in PBS and filtered through a 0.22 μm syringe filter. FC was added to the 100 μM curcumin solution to make a 10% (w/v) solution mixture. The mixture was adjusted to pH 7.4 by the addition of 1 M Tris-HCl.

Curcumin-loaded FC/FI (FC/FI-Cur) hydrogel was prepared in an analogous way. Curcumin was dissolved in DMSO at 10 mM under stirring until completely dissolved. Next, curcumin solution was diluted to 100 mM in PBS and filtered through a 0.22 μm syringe filter. FI was mixed with the curcumin solution in order to reach a final concentration of 1% (w/v). Once dissolved, an appropriate amount of FC was added to the mixture to reach a final concentration of 10% (w/v) and adjusted to pH 7.4 by the addition of 1 M Tris-HCl.

2.4. Characterization of the modified chitosan

2.4.1. Nuclear magnetic resonance (NMR) spectroscopy

^{1}H NMR spectra were performed on a Bruker-500 at 500 MHz. Chemical shifts are reported in ppm versus deuteroxide as an internal standard. FC and Fmoc-G were dissolved in D_2O under stirring, while CS was dissolved in 95% D_2O with 5% CD_3COOD.

2.4.2. UV–vis spectroscopy

UV–Vis spectra were recorded on a Uv-2450/2250 (Shimadzu) spectrophotometer. To this end, FC and Fmoc-G were diluted in deionized water. For the insoluble chitosan, 10 mg of powder was dissolved in deionized water under stirring for 5 min and the solution was centrifuged to obtain the supernatant for UV–Vis measurement. The absorbance of CS, Fmoc-G and FC solutions was measured after shaking the samples from wavelength 200–400 nm.

2.4.3. Rheological tests

A Kinexus Pro rheometer (Malvern) equipped with a 10 mm-diameter parallel plate geometry was used to test the mechanical properties of the hydrogels at 25 °C. 500 μL of each sample were gently placed with a gap of 0.5 mm. Frequency sweeps were performed to collected storage (G′) and loss (G″) moduli at a constant strain amplitude of 0.5% and at oscillation frequencies from 0.1 to 10 Hz. Amplitude sweeps were performed and each hydrogel was strained at a constant oscillation frequency of 1 Hz and variable applied strain from 0.1 to 1000% until failure. Time sweeps were performed at a constant strain amplitude of 1% and a constant oscillation frequency of 1 Hz with variable applied time.

2.4.4. Scanning electron microscopy (SEM)

The morphology of all hydrogel was monitored by a Zeiss Ultra 55 Field Emission Scanning Electron Microscope (Zeiss) with an accelerating voltage of 5 KV. Before the observation, the hydrogels were cut in liquid nitrogen to reveal the cross-sectional surface and lyophilized. Next, the hydrogel samples were sputter-coated with goat and examined using SEM.

2.5. Study of self-healing property

2.5.1. Macroscopic self-healing experiments

Macroscopic self-healing experiments were chosen to evaluate the self-healing performance of FC and FC/FI hydrogels. One piece of the hydrogel (both FC and FC/FI) was stained with rhodamine, respectively. The mixture was transferred to the columnar mold and incubated at 25 °C for 24 h to get the columnar hydrogel. Next, each gel was cleaved into three pieces and put together and placed in the mold for 24 h. The self-healed columnar hydrogel could support the weight of itself, and then the morphological changes of recombined hydrogel were observed to evaluate the self-healing performance.

2.5.2. Quantitative self-healing experiments

A dynamic oscillatory rheology assay was performed to quantitatively evaluate the self-healing property of the hydrogel. Briefly, a strain amplitude cyclic step test alternating from small strain ($\gamma = 0.5\%$) to large strain ($\gamma = 600\%$) with a fixed frequency of 1 Hz for 120 s at 25 °C. For each measurement, 5 cycles were carried out, and the changes of storage (G′) and loss (G″) modulus with strain amplitude and time were recorded. In addition, the recovery time was verified by recording the storage (G′) and loss (G″) modulus, immediately after the fracture of each gel strained from 0.1% to 1000%.

2.5.3. Circular dichroism (CD)

Information of Fmoc-G, FI and FC arrangements were recorded using a Chirascan spectropolarimeter (Applied Photophysics, UK) in a range of wavelength of 190–260 nm with a bandwidth of 1 nm at 25 °C. Solutions of each sample were loaded into a 0.1 cm cuvette and degassed, and the data were averaged across three scans.

2.5.4. Fluorescence spectroscopy

Interactions between the fluorenyl groups of the FC and FI molecules were investigated on a FS5 (Edinburgh) fluorescence spectrophotometer. Fluorescence emission spectra were measured with excitation at 265 nm and emission data range from 290 nm to 600 nm.

2.5.5. Fourier transform infrared (FTIR) analysis

Fmoc-G, CS, FC, FC hydrogel and FC-FI powder were characterized by a VERTEX 70 infrared spectrometer (Bruker) with 16 scans at a resolution of 4 cm^{-1} over a wavenumber range of 4000–400 cm^{-1}. Before the measurement, all samples were dried and compressed into KBr pellets.

2.5.6. Atomic force microscopy (AFM)

The morphology of FI was investigated using a Multimode-V (Bruker) atomic force microscope (AFM) operated in ScanAsyst mode in air. Briefly, samples were diluted with deionized water to a concentration of 0.2% (w/v) or 0.05% (w/v). 3 μL aliquot of the diluted solution was allowed to spotted onto a freshly cleaved mica surface and then dried in an electronic drying cabinet for 12 h.

2.6. In vitro drug release study

The standard curve line of curcumin was constructed by recording the absorbance of serial dilutions of curcumin solution of known concentration (3.125, 6.25, 12.5, 25, 50 μmol/L) at 429 nm. FC-Cur and FC/FI-Cur hydrogels were prepared as described above. 500 μL hydrogels were placed into 1 mL physiological saline solution at 37 °C with shaking at 100 rpm. At the preplanned time point, an aliquot of the released mixture (1 mL) was withdrawn and replaced with an equal volume of fresh media. The concentrations of curcumin released from hydrogels of the mixture was qualified the UV–vis spectrophotometer (Shimadzu). Each experiment was carried out in triplicate, and average values were plotted.

2.7. DRG cell culture

2.7.1. DRG isolation and culturing

FC, FC/FI and FC/FI-Cur hydrogels were coated on glass slides and sterilized by UV light for 30 min, which were correspondingly defined as the experimental groups: FC, FC/FI and FC/FI-Cur. Whole DRGs with redundant roots were isolated under a stereomicroscope from postnatal Sprague-Dawley rats (1–3 days, P1), supplied by the Laboratory Animal Center of Southern Medical University, China. The residual nerve roots of DRGs were removed using surgical forceps. DRGs were collected and placed on hydrogels-coated glass slides, which were put in a 24-well plate and culture with neurobasal medium containing 2% B27 (Nest Biotechnology Co., Ltd.), 0.3% L-glutamine (Gibco, USA), 100 ng/mL neural growth factor (NGF, Peprotech, USA) and 1% penicillin-streptomycin (Nest Biotechnology Co., Ltd) in a 37 °C incubator with 5% CO_2 and 92% humidity for 7 days. The medium was changed every 2 days.

2.7.2. Myelination study

FC, FC/FI and FC/FI-Cur hydrogels were coated on glass slides and sterilized by UV light for 30 min. Whole DRGs with redundant roots were isolated under a stereomicroscope from postnatal Sprague-Dawley rats (1–3 days, P1). The residual nerve roots of DRGs were removed using surgical forceps. DRGs were collected and placed on hydrogels-coated glass slides, which were put in a 24-well plate and culture with neurobasal medium containing 2% B27, 0.3% L-glutamine, 100 ng/mL NGF and 1% penicillin−streptomycin in a 37 °C incubator with 5% CO_2 and 92% humidity. Seven days after plating, 50 μg/mL ascorbic acid

(Nest Biotechnology Co., Ltd.) was added to the medium of the DRGs to trigger myelination by the endogenous SCs. Cells receiving ascorbic acid were fed with the same media thrice per week.

2.8. In vivo spinal cord injury

2.8.1. Animals

Young adult female SD rats (220–250 g) were purchased from Laboratory Animal Center of Southern Medical University, China, and housed in temperature and humidity-controlled animal quarters under a 12 h light/dark cycle. All animal procedures were approved by the Animal Ethics Committee of Jinan University and raised in SPF laboratory animal room.

2.8.2. Spinal cord transection and animal care

The rats were divided into four groups (18 rats per group) for *in vivo* study: (1) CTRL group: physiological saline solution was injected into the lesion area. (2) FC group: FC hydrogel was implanted into the lesion area. (3) FC/FI group: FC/FI hydrogel was implanted into the lesion area. (4) FC/FI-Cur group: FC/FI-Cur hydrogel was implanted into the lesion area. The SD rats were anesthetized with 2% pentobarbital sodium (30 mg/kg body weight) via intraperitoneal injection. Laminectomy was performed to expose the thoracic (T9-T10) vertebrae under an operating microscope. A #11 blade was used to vertically cut the endorhachis, and a 2 mm segment of the spinal cord at the T9 level was removed, and any residual nervous tissue was removed at the transection site. After hemostasis, about 10 μL hydrogel scaffolds or equal volume physiological saline solution were injected into the gaps at the lesion sites, and endorhachis was sutured with #7-0 silks. The muscles and skin were closed with sterile sutures in separate layers. After the surgery, the experimental rats routinely received antibiotics (penicillin, 50.000 U/kg/d) intramuscularly for 5 days and manual micturition twice a day until their automatic micturition function was recovered.

2.9. Immunofluorescence staining

2.9.1. Antibodies

The detailed antibody information was provided in Table 1.

2.9.2. Experiment section

The cells were determined using immunofluorescence staining with corresponding antibodies following the standard protocols. Briefly, cells were fixed by 4% paraformaldehyde in PBS for 2 h, rinsed with PBS (3 × 10 min), permeabilized, and blocked with 0.1% Triton X-100 and 10% normal donkey serum in PBS for 30 min. Cells were incubated with primary antibodies against anti-NF200 and anti-S100 antibodies with DRG culture samples, and anti-NF200 and anti-myelin basic protein (anti-MBP) antibodies with myelinating SCs for 2 h at 25 °C, followed by secondary antibodies conjugated to donkey anti-mouse IgG 647 (Millipore, 1:1000) and donkey anti-rabbit IgG 555 (Millipore, 1:1000) for 1 h. The cells were then rinsed with PBS (3 × 10 min) and finally covered with coverslips and Fluoro-Gel II with DAPI (Electron Microscopy Sciences, England) for 20 min.

The rats were anesthetized with an overdose of 1% pentobarbital sodium (30 mg/kg, body weight) and the spinal cord were excised, fixed at 4 °C in fixing solution overnight. The tissue was then placed in 20% sucrose solution (with 0.1 M PBS) and 30% sucrose solution (with 0.1 M PBS) overnight in turn until the tissue sank to the bottom. The spinal cord tissue, including the injury region, was then embedded in an OCT compound (Sakura Finetek). The specimens were placed in a −80 °C refrigerator to ensure appropriate cutting temperature, and sliced longitudinally to produce 15 μm sections. The sections were washed with PBS (3 × 10 min) and blocked with 0.1% Triton X-100 and 10% normal donkey serum in PBS for 1 h. The sections were incubated overnight with primary antibodies at 4 °C overnight. Next, the sections were washed with PBS (3 × 10 min) and incubated with secondary antibodies for 1 h in the dark at 25 °C. The sections were then rinsed with PBS (3 × 10 min) and finally covered with coverslips and Fluoro-Gel II with DAPI (Electron Microscopy Sciences, England) for 20 min. The images were acquired using an LSM700 confocal microscope (Zeiss, Germany).

2.9.3. Quantitative reverse transcription polymerase chain reaction (RT-PCR) analysis

Total RNA was extracted from DRGs cultured for 14 and 30 days using the TRIzol (Ambion, USA) method. RNA concentration was analyzed spectrophotometrically using a NanoDrop 2000C instrument (Thermo Scientific, USA). Prime Script Kit (Takara, Japan) was used for cDNA synthesis was prepared from total RNA (500 ng) using according to the manufacturer-specified procedure. RT-PCR was performed using SYBR Premix EX Taq II (TakaRa, Japan) with the primers listed in Table 2, and investigation was conducted for a mixture (10 μL) of SYBR Premix Ex Taq II (5 μL), diluted cDNA (1 μL), forward primers (0.2 μL), reverse primers (0.2 μL) and deionized water (3.6 μL).

2.9.4. Motor evoked potential (MEP) detection

MEP testing was performed on a BL-420 Data Acquisition Analysis System (TECHMAN SOFT, China) to record the motor nervous system recovery of each group under differential treatments (six rats per group). The rats were anesthetized with 2% pentobarbital sodium (30 mg/kg body weight) via intraperitoneal injection.

The cerebral cortex was exposed, with the stimulation electrodes touching the cortex, which included a positive electrode and a negative electrode. The recording electrodes were inserted into the gastrocnemius muscle of the contralateral hind limbs. The ground line was positioned between the stimulating and recording electrodes. The latency and amplitude from the negative peak to the adjacent positive peak were examined by MEP testing.

2.9.5. Functional behavioral evaluation

The Basso-Beattie-Bresnahan (BBB) locomotor assessment was performed to evaluate the mobility of hind limbs in the rats after SCI (six rats per group). At a specific point in time, each experimental animal was placed in an open field and recorded the BBB score according to the functional evaluation criteria of the SCI proposed by Basso et al.

Table 1
Information of antibodies utilized in the study.

Name	abbreviation	host	dilution	company
anti-CD68	CD68	mouse	1:300	Abcam
anti-liver arginase	ARG1	rabbit	1:500	Abcam
anti-S100	S100	rabbit	1:500	Abcam
anti-neurofilament200	NF200	mouse	1:500	Sigma
anti-glial fibrillary acidic protein	GFAP	mouse	1:500	Sigma
anti-myelin basic protein	MBP	rabbit	1:300	Millipore
anti-mouse IgG 647		donkey	1:1000	Millipore
anti-rabbit IgG 555		donkey	1:1000	Millipore

Table 2
Information of Primer in this study.

ID	primer name	Sequence
MBP	Forward Primer	TCACAGCGATCCAAGTACCTG
MBP	reverse primer	CCCCTGTCACCGCTAAAGAA
AKT1	Forward Primer	ATGAACGACGTAGCCATTGTG
AKT1	reverse primer	TTGTAGCCAATAAAGGTGCCAT
ERK2	Forward Primer	GGTTGTTCCCAAATGCTGACT
ERK2	reverse primer	CAACTTCAATCCTCTTGTGAGGG
GAPDH	Forward Primer	TGGCCTTCCGTGTTCCTAC
GAPDH	reverse primer	GAGTTGCTGTTGAAGTCGCA

2.10. Statistical analysis

Data are expressed in the form of mean ± standard deviation. Differences between groups were evaluated using one-way analysis of variance followed by Dunnett's or Bonferroni's *post hoc* test. Statistical significance was considered when $p < 0.05$ (*), $p < 0.01$ (**), and $p < 0.001$ (***).

3. Results and discussions

The 9-fluorenylmethoxycarbonyl (Fmoc) strategy is widely used in peptide synthesis in biomedical applications [24]. In the current study, we presented a hybrid hydrogel with intrinsic healing property from two Fmoc-containing biomaterials, defined as FC and FI, respectively. As shown in Fig. 1, Fmoc-glycine (Fmoc-G) was chemically conjugated onto chitosan using EDC/NHS as activators. The chemical structure was analyzed by ^{1}H NMR (Fig. 1D). Characteristic chemical shifts corresponding to proton signals of the aromatic Fmoc groups at 7.45–7.94 ppm appeared in FC as compared to that of unmodified CS, confirming the successful conjugation of Fmoc to CS molecules. The grafting yield, determined from integral values of the proton peak of the Fmoc group, was approximately 14.4%. The dissolvability of CS was greatly improved after modification, which was probably ascribed to the fact that the introduction of Fmoc moieties destroyed the hydrogen bonds of CS. The adsorptions of CS, Fmoc-G and FC solutions were monitored using UV-spectroscopy (Fig. 1E). Similar to Fmoc-G, FC exhibited a peak centered at 264 nm in the absorption spectrum, corresponding to the absorbance of the Fmoc group, with two shoulders appearing at 288 and 298 nm.

Fmoc-peptide has attracted a lot of attention in biological applications, involving in tissue engineering, drug delivery, bio-imaging and biosensors [25]. In this study, we designed a Fmoc-diarginine (Arg-Arg) modified by a pentapeptide IKVAV (Ile-Lys-Val-Ala-Val) at the C-terminus (Fig. 1C). IKVAV derived from laminin was introduced because of the ability of mimicking some neurite outgrowth activities of intact laminin [26].

The properties of the amino acids play a key role in the solubility and physicochemical properties of the resultant peptides [27,28]. Two arginines were specially inserted between Fmoc moiety and the IKVAV motifs in order to obtain positive charges. The zeta potential of FI was 1.92 at physiological pH. Therefore, electrostatic repulsions of FI monomers in an aqueous solution allowed FI molecules to be well-dissolved in water for prolonged periods (Fig. 2A) and a low storage modulus (G′) was observed (Fig. 2B). Meanwhile, the G′ value was found

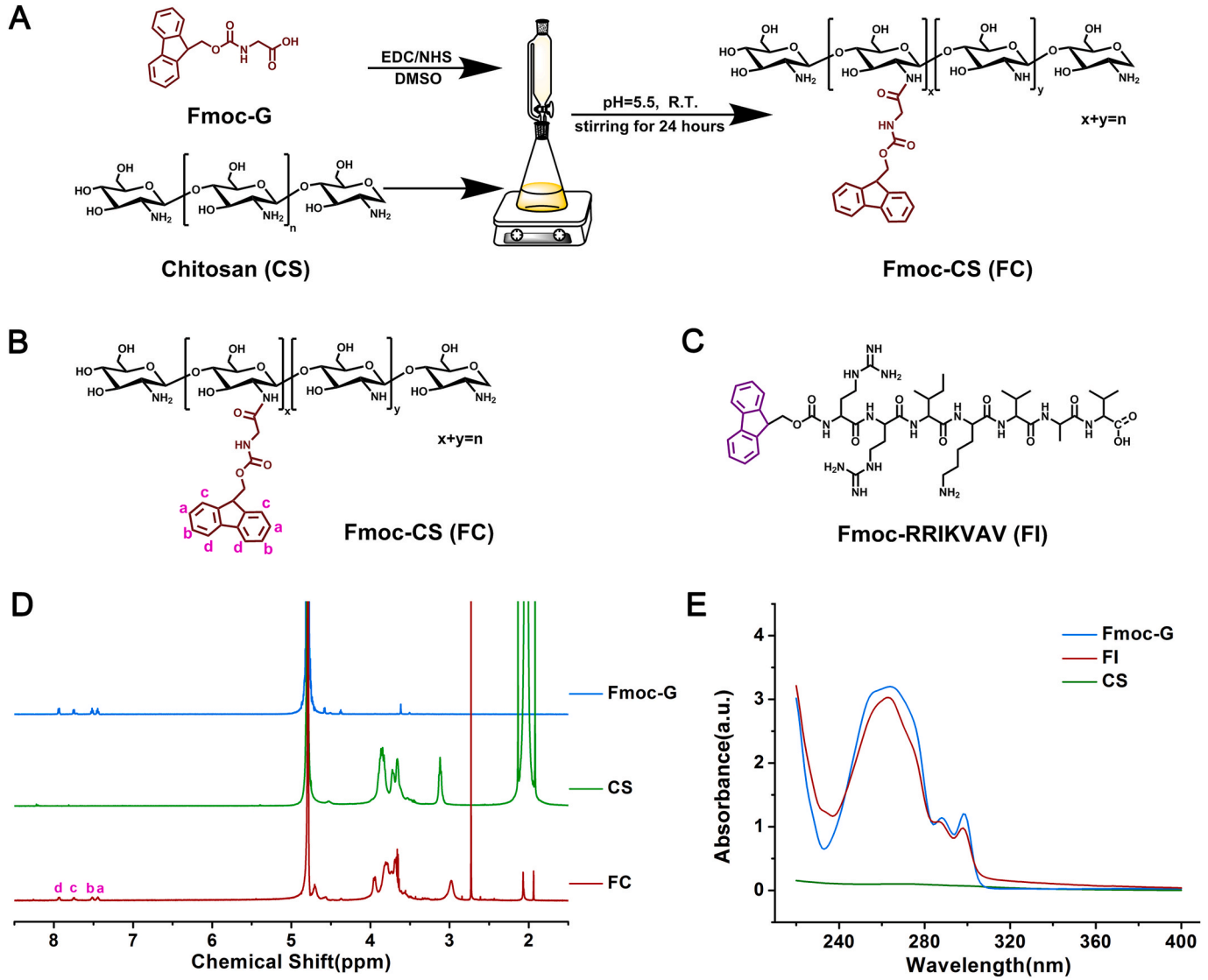

Fig. 1. Preparation of chemicals for hydrogels. (A) Synthetic route toward FC by grafting Fmoc-G onto chitosan using EDC/NHS as activators. (B) Chemical structure of FC. (C) Chemical structure of FI. (D) ^{1}H NMR spectra and (E) UV–Vis spectra of various chemicals.

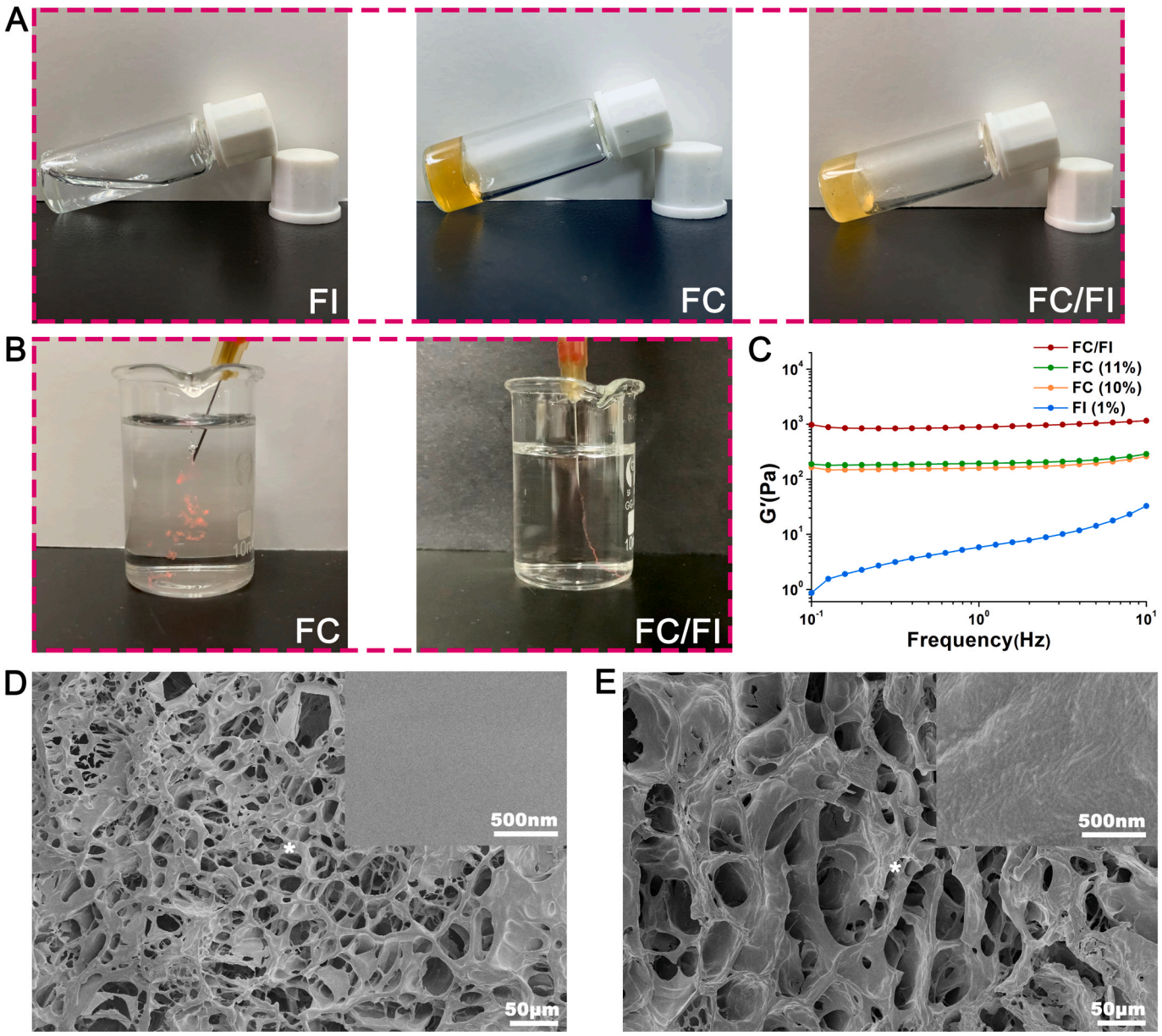

Fig. 2. Appearance and related properties of FC/FI hybrid hydrogel. (A) FI solution was liquid while FC and FC/FI formed hydrogels. (B) The storage modulus (G′) of FI, FC and FC/FI. (C) Images showing large fragments after FC injection whereas integrated hydrogel was observed after FC/FI injection. (D) SEM image of FC hydrogel. (E) SEM image of FC/FI hydrogel. Images of a higher magnification of the "*" place were presented in the upper right corner of (D) and (E).

to increase with an increase in shear rate, showing a shear thickening behavior. It was well known that Fmoc-peptides could self-assemble into stable secondary structures (α-helix, β-sheet, or random coil), eventually forming hydrogels composed of various supramolecular structures such as nanospheres, nanotubes, micelles, fibrils, tapes [25,29,30]. In this study, a weak hydrogel was formed when exposing 1% FI aqueous solution to PBS. Fragments composed of fibrils were obtained after lyophilization (Fig. S1). AFM observation showed that FI of a high concentration (0.2%) appeared as networks of short picks, whereas FI of a low concentration (0.05%) became scattered particles and short picks (Figs. S1C and S1D). Aggregation and entanglement initiated by π-π stacking of the Fmoc moieties occurred during shearing treatment, which might be responsible for the shear thickening behavior [31].

The viscous and non-flowable solutions were obtained by freshly dissolving FC in water and further adding FI. It was interesting that FI's addition significantly increased G′ of the resultant hybrid. In order to eliminate the influences of increased concentration, 11% (w/v) FC was prepared, which showed a slightly higher G′ than 10% FC. These results indicated that a certain structure was probably formed between FC and FI, contributing to the network of the hybrid hydrogel. Fmoc moieties in FC and FI provided abundant hydrophobic and π-π stacking interactions of the fluorenyl rings. These unique and strong interactions were expected to drive the aggregation of FC and FI by serving as physically cross-linked points in a kinetically rapid and thermodynamically rigid manner in the hybrid hydrogel. SEM images showed that FC and FC/FI hydrogels were both composed of interconnected pores with pore diameter ranging from 20 to 60 μm. Images of higher magnification showed that the pore walls of FC were smooth while those of FC/FI were composed of fibrils and spherical bumps, suggesting that FI were buried within the FC bulk.

Both FC and FC/FI was injected through 26G needle as shown in Fig. 2B. The π-π stacking interactions were dynamically reversible, which endowed the hybrid hydrogel with good injectability. Large fragments were observed after FC injection into PBS whereas integrated

linear hydrogel was formed after FC/FI injection. We speculated that FI nanoparticles and short sticks formed via self-assembly when exposing to PBS interacted with FC macromolecules and further assisted the integration of the hybrid hydrogel.

Pieces cut from FC hydrogel and FC/FI hybrid hydrogel were both autonomously merged into an integrated hydrogel with a junction upon being placed close together (Fig. 3). However, a seam between two FC parts was visible in SEM pictures, although the two separate pieces connected together (Fig. 3C). By contrast, it was hard to distinguish the interface between the two FC/FI separate pieces (Fig. 3D). These observations supported the idea that FC/FI hybrid hydrogel could heal themselves automatically to form an integrated structure without additional stimuli.

Rheological strain sweep measurements were conducted on the hydrogels to quantitatively investigate the responsive behavior upon external strains. As shown in Fig. 4, both G′ and G″ values of the FC/FI hydrogel maintained highly constant when the applied strain increased from 0.1 to 100%. Further increasing the strain to 200% caused a drop of G′ value but an increase of G″ value with a crossover point occurring at around 600%. This observation suggested that the hydrogel network got ruptured and became a sol state due to the severe dislocation of cross-linking points [32]. However, the rheological properties were almost fully recovered upon applying a 1% strain immediately ($\gamma = 1000\%$) (Fig. 4A). Similarly, the rheological properties of FC hydrogel could also be recovered when a 1% strain was applied immediately after the gel failure ($\gamma = 1000\%$) (Fig. 4B). A drop of G′ value but an increase of G″ value with a crossover point occurring at around 200% occurred following a strain of 100% applied to FC hydrogel.

The strain-induced damage and healing were furthermore evaluated by continuous step change of oscillatory strain between 600% and 1% under the same frequency of 1 Hz. Before applying a high shear rate, FC/FI hydrogel was able to maintain a colloidal state of a viscosity at ~900 Pa. A large dynamic strain of 600% decreased the G′ of the hydrogel from the original value of ~900 Pa–~20 Pa. Such a high strain would destroy the hydrogel structure as indicated above. Following maintenance of large strain for 120 s, G′ returned quickly to the initial value after applying a low strain of 1%, suggesting the hydrogel structure was probably recovered. The finding of damage of the self-healing hydrogel at a high shear strain and healing at a low strain was in good agreement with the healing process observed above in photographs. FC/FI hydrogel showed good and repeatable circulation in rheological properties after the continuous step strain, with ~88% recovery of G′ value after 5 circles. On the contrary, the recovery sustainedly decreased after applying the continuous step strain to FC hydrogel despite the apparent healing, with ~70% recovery of G′ value after 5 circles (Fig. 3A). These results showed that the addition of FI enhanced the resistance of FC hydrogel to sol-gel transition and possessed good self-healing property.

These results showed that the interactions between FC and FI played a vital role in the injectable and self-healing performances of the resultant hybrid hydrogel. More studies were thus performed to investigate the underlying mechanisms. The nature of the peptidic tail has been documented to have a pronounced effect on the self-assembly behavior of Fmoc-peptide [33]. The hydrophobic Isoleucine, Valine and Alanine in the pentapeptide IKVAV drove the self-assembly process of FI via hydrophobic interactions in addition to π-π stacking interactions. A strong negative band located at around 199 nm in the CD spectra indicated of the random coils (Fig. 5A), which was responsible for the nanoparticles and short sticks as shown in the AFM images

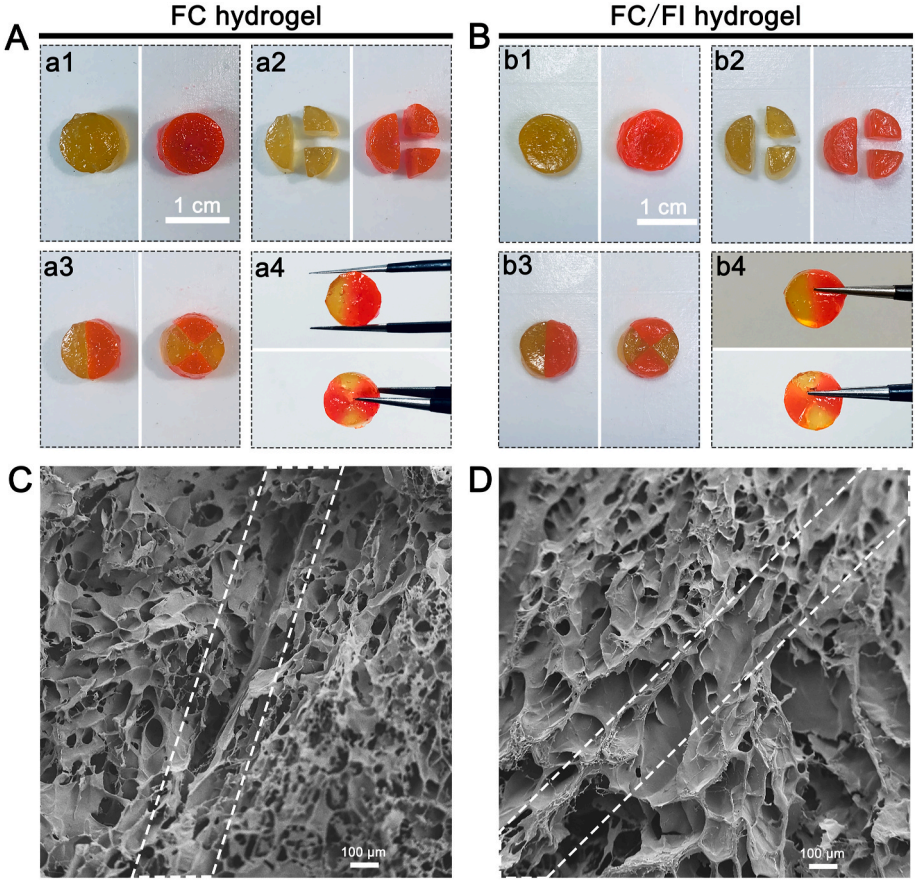

Fig. 3. Self-healing behavior of round hydrogels with different colors for a distinguishable interface. Both the pieces from FC hydrogels (A) and FC/FI hydrogels (B) could aggregate into one hydrogel. (C) and (D) were SEM images of aggregated hydrogels of FC and FC/FI. The frame of dotted lines showed the interfaces of the pieces. Scale bars were 100 μm in (C) and (D).

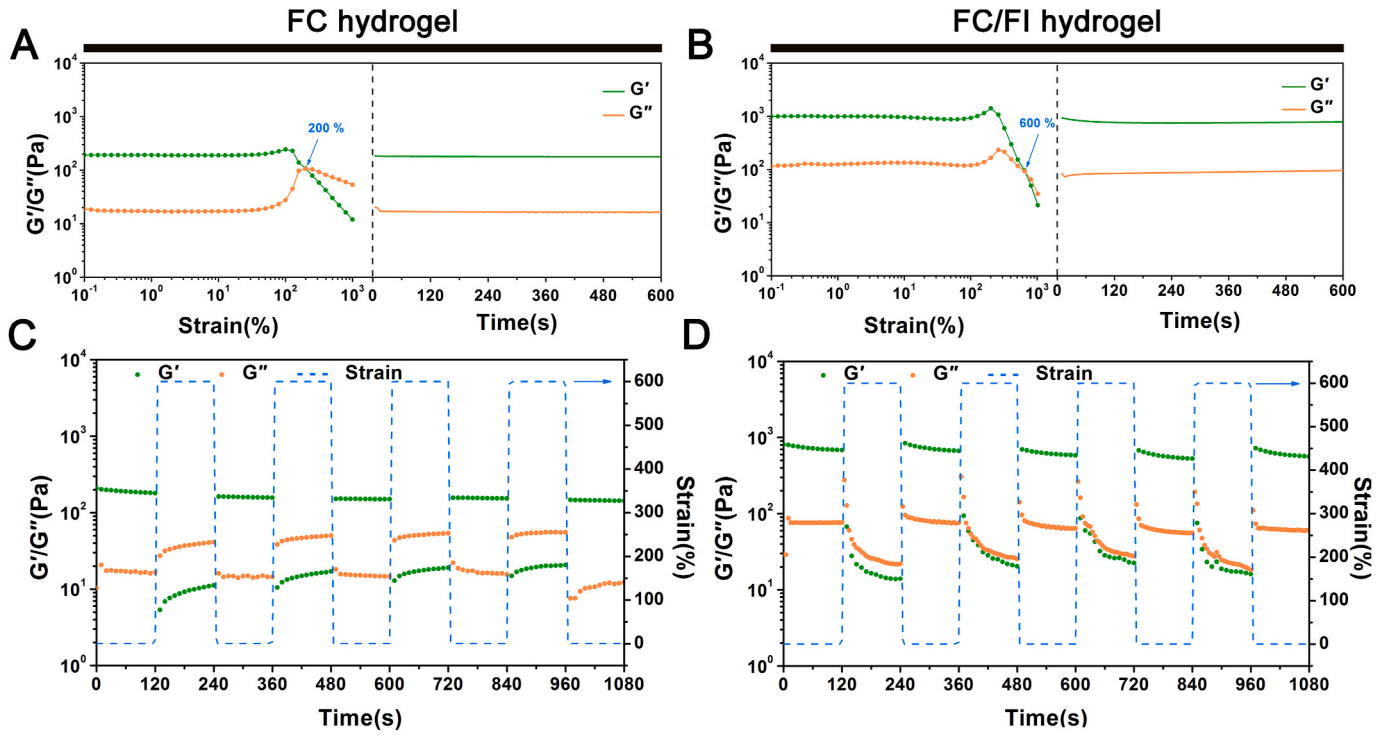

Fig. 4. Investigation on self-healing behaviors. The modulus (G′ and G″) changes of FC hydrogel (A) and FC/FI hydrogel (B) at 1 Hz upon enhanced external strains at 25 °C (left) and an instantaneous recovery from the 1000% strain deformation (right). The damage-healing property of FC hydrogel (C) and FC/FI hydrogel (D) demonstrated by the continuous step strain (1% strain→600% strain→1% strain) measurements at a fixed time interval of 120 s at 25 °C.

(Fig. S1). Similarly, a characteristic negative band at around 199 nm was observed in the spectra of FC/FI hybrid, indicating that FC showed less impact on FI self-assemble process in the dilute status (0.01%). Fluorescence spectroscopy was employed to monitor the molecular environment of FC, FI and FC/FI hybrid fluorenyl moieties (Fig. 5B). In order to allow comparison of the relative intensity, all the fluorescence spectra of the compounds were normalized by setting the emission maximum to 1. At a low concentration of 1%, both FC and FI molecules should be in their ionized form in the clear solutions. The emission maximum at 312 nm was ascribed to the fluorenyl fluorescence of FC and FI in their monomeric state [33,34]. The main fluorescence peak shifted to 318 nm at a concentration of 10%, in which case FC, FI, and FC/FI were hydrogels. It was documented that the emergence of red shift with respect to the monomer peak was indicative of the presence of excimers (excited dimers) of fluorenes, suggesting stronger interactions between the Fmoc moieties [34]. A weak shoulder was observed at around 380 nm in FI spectra (arrows in Fig. 5B), which was documented to be associated with the formation of micelles by Sadownik JW et al. The fluorenyl moieties were confined inside the supramolecular structure in a parallel manner [35]. Meanwhile, several photoluminescence peaks centered at 425–575 nm were detected for FC, FI, and FC/FI hydrogels but no fluorescence emission signals were observed for 1% FC and FI solutions. The observation of photoluminescence peaks indicated of the presence of extensive J-aggregates formed by multiple aromatic groups of the fluorenyl and phenyl rings through π-stacking interactions [36].

As compared to CS, both FC powder and hydrogel showed a new band at 744 cm^{-1} in the FTIR spectra, which was assigned to the characteristic out-of-plane bending vibration ($\gamma_{=C-H}$) of Fmoc moieties, confirming the successful conjugation of Fmoc-G to CS (Fig. 5C). Meanwhile, the absorption peak of N–H stretching vibration of CS at 3445 cm^{-1} associated with intramolecular hydrogen bonds was found to red shift to 3431 cm^{-1} in FC powder. This observation indicated that Fmoc conjugation attenuated the intramolecular hydrogen bonds of CS, thus improving the solubility of CS [37]. Increased red-shift was observed in FC hydrogel and FC/FI hydrogel, which might indicate that the π-π interactions of the fluorenyl moieties further attenuated the intramolecular hydrogen bonds of CS.

Collectively, the analyses above revealed that π-π stacking interactions of Fmoc moieties were the main driving force behind FC/FI gelation. A schematic illustration outlining the mechanism for injectable and self-healing capabilities of FC/FI hydrogel was provided (Fig. 5D). The abundant π-π stacking interactions of the fluorenyl rings in Fmoc moieties served as physically cross-linked points of FC hydrogel. The addition of FI, as diluted nanoparticles and dissolved molecules, further provided intermolecular π-π stacking interactions with FC, resulting in more cross-linked points and therefore enhancing the mechanical strength of the resultant hybrid hydrogel. The intrinsic hydrophobicity of Fmoc moieties would promote the hydrophobic affinity interactions, which were also expected to serve as physically cross-linked points in FC/FI hydrogel. Since non-covalent interactions were dynamically reversible, the hybrid hydrogel was imparted with good injectability and self-healability. The injectability facilitated the fabrication of hydrogels with specific shapes and administration through a minimally invasive manner, whereas hydrogels integrated with self-healing ability benefit long-term use as well as enhanced durability to support regenerating axons and migrating cells in the lesion. Curcumin was encapsulated within the hybrid hydrogel, which could be released in a sustainable pattern. Several studies focus on synthesis of polymeric hydrogel of self-healing properties for treating SCI [38]. Advances in molecular science make it feasible by creating complicated molecular structures in order for multiple functions. Potentially toxic and recalcitrant chemicals, however, were involved in the synthesis [12]. The hydrogel we developed took advantage of the versatility of Fmoc-functioned molecules and exhibited excellent performance, which was highly promising for biomedical applications.

Encouraged by these promising results on materials science, we investigated the applications of hydrogel in repairing SCI. Cur was encapsulated in FC and FC/FI hydrogels before gelation. Most of Cur was buried within the hydrogel matrix while some of Cur adsorbed on the wall of the hydrogels, appearing as particles (arrows in Fig. 6A and B).

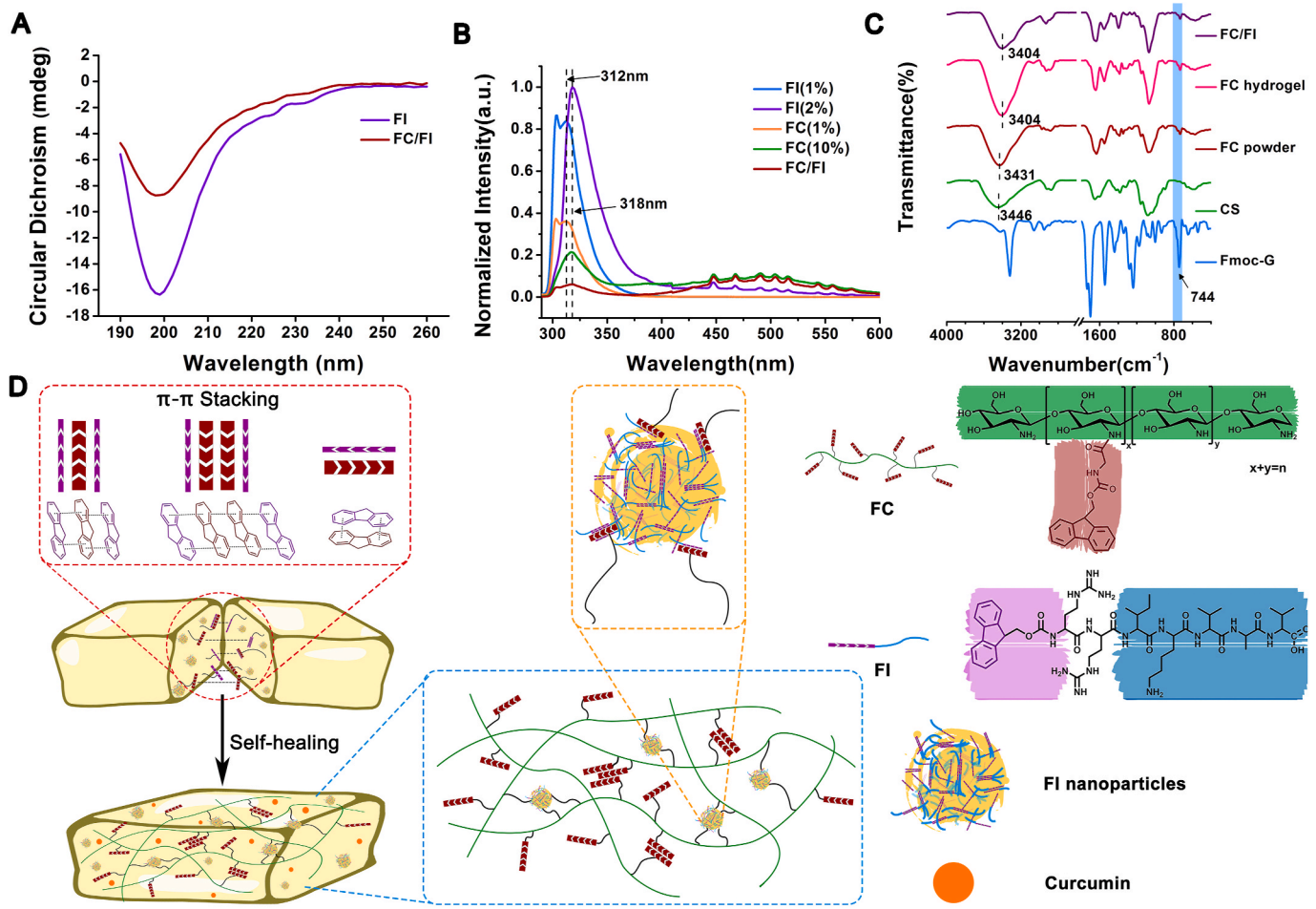

Fig. 5. Investigation on the interactions between FC and FI. (A) CD spectra. (B) normalized fluorescence emission spectra. (C) FTIR spectra. (D) Proposed schematic mechanism for dynamic interactions between FC and FI for self-healing behavior of FC/FI hybrid hydrogel. Curcumin was encapsulated within the hydrogel as a model drug for therapeutics.

Cur showed a slow release during the 7-day period. The relatively quick release within the first 12 h was ascribed to the Cur on the wall. Similar to our previous study, FC/FI hybrid hydrogel had a higher mechanical strength compared to FC hydrogel, which inhibited Cur mobility within the matrix and thus slowed down the release [10]. The growth of DRG spheres on the hydrogels made of FC, FC/FI and FC/FI-Cur was studied at first. DRG spheres were well attached to the hydrogels with long axon outgrowth and SC migration away from the DRG spheres after 7 days (Fig. 6D and Fig. S2). The pentapeptide IKVAV was demonstrated to promote neurite outgrowth [26], which was responsible for the significantly longer neurites on FC/FI than those on FC. The addition of Cur further accelerated neurite outgrowth, resulting in an average neurite length of 2047 ± 231 μm on FC/FI-Cur hydrogel (Fig. 6F a). Meanwhile, SC migration away from DRG spheres was observed as determined by $S100^+$ immunostaining, especially on FC/FI-Cur hydrogel (Fig. 6F b). Images of a higher magnification showed that SCs spread along the axons in a linear end-to-end manner (Fig. S2). SCs were well dispersed on FC and FC/FI hydrogels (indicated by the arrow in Fig. S2), but those on FC/FI-Cur hydrogel were not. Such an observation indicated that Cur enhanced the interactions between SCs and neurites, which was confirmed by quantifying the percentage of SCs attached to DRG neurites (Fig. 6F c).

Myelination of neurites was assessed by immunochemical staining of anti-NF200 and anti-MBP antibodies after 1 month. As shown in Fig. 6E, MBP signals strongly overlapped with neurites, as indicated by the single optic section confocal images with the Z-stack. MBP mRNA expression on these hydrogels was tested after culturing DRG for 1 month. Cells on FC/FI-Cur hydrogel showed the highest expression level, significantly higher than those of the other two groups ($p < 0.001$). No significant differences in terms of MBP expression level were observed between FC hydrogel and FC/FI hydrogel. Meanwhile, expressions of ERK2 and AKT1 mRNA were tested, both of which were involved in many biological processes, such as metabolism, cell proliferation, and growth. Incorporating FI into FC hydrogel resulted in significantly higher expression levels of ERK2 and AKT1 mRNA ($P < 0.05$). Controlled release of Cur further promoted the expressions of ERK2 and AKT1 mRNA. These observations indicated enhanced survival of neurons and SCs on FC/FI and FC/FI-Cur hydrogels.

Traumatic spinal cord injury (SCI) triggers an inflammation with an invasion of abundant inflammatory cells, which hinders neural regeneration. Therefore, the regulation of inflammatory responses in the early stage of SCI has been a therapeutic target of widespread concern [39]. In the current study, a general marker (CD68) and a specific marker for the anti-inflammatory phenotype (ARG1) of macrophage/microglia, the main inflammatory cells in the lesion site, were detected by immunocytochemistry in order to assess different subsets of the activated macrophage/microglia after SCI (Fig. 7 and Fig. S4). Numerous $CD68^+$ cells invaded within hydrogels in the lesion site 2 weeks after SCI. Meanwhile, most of these cells were positively stained with ARG1. However, accumulation of $CD68^+$ cells only occurred in the connective tissues in the CTRL group with no implantation performed. Statistical analysis showed that the number of $ARG1^+$ cells in the lesion sites increased in the order of CTRL, FC hydrogel, FC/FI hydrogel and FC/FI-Cur hydrogel (Fig. 7I). Pairwise comparisons of FC/FI-Cur with other groups indicated

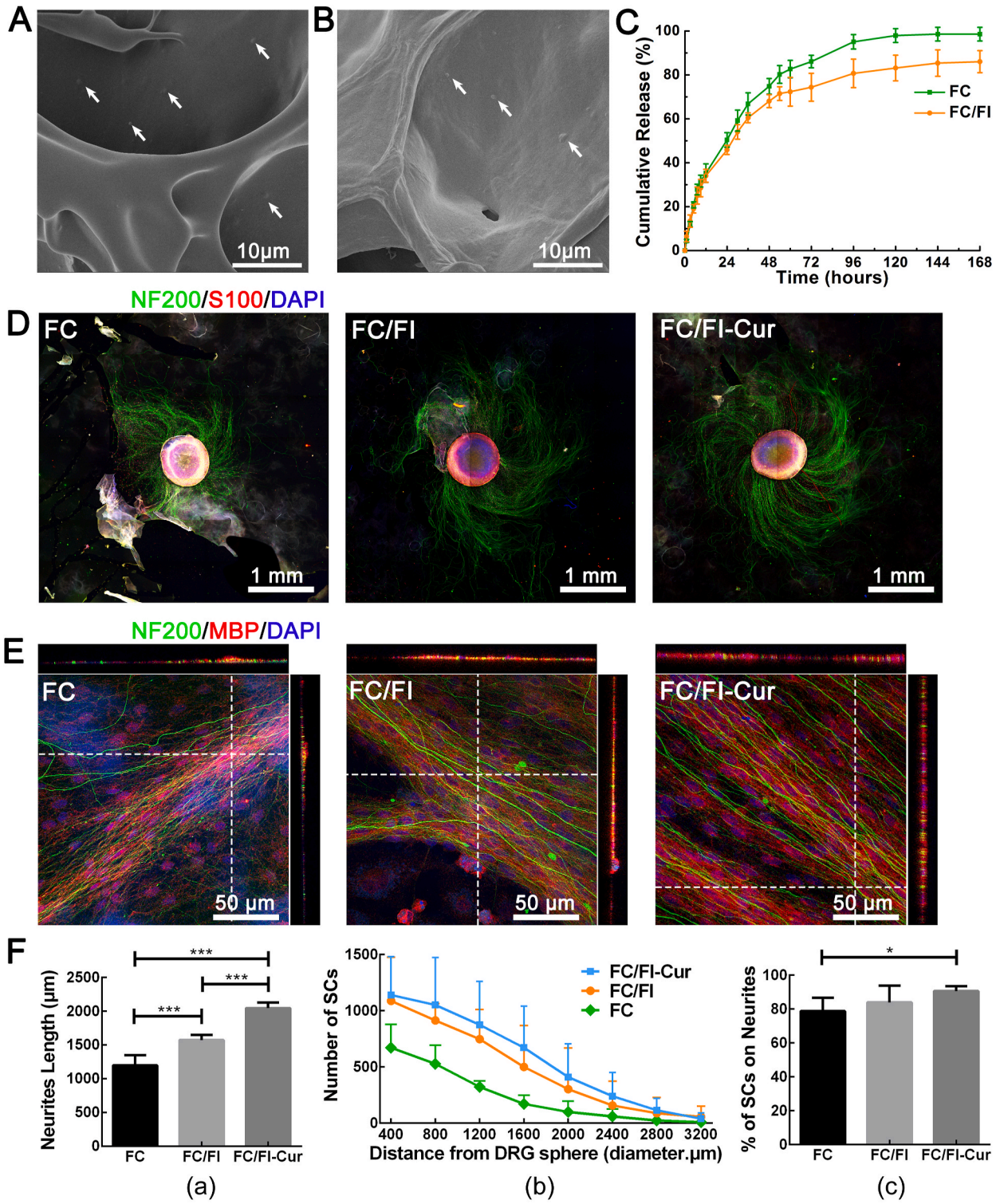

(caption on next page)

Fig. 6. Investigation on DRG growth. (A) and (B) were SEM images of Cur-loaded FC and FC/FI hydrogels, respectively. (C) Cur release curves from FC and FC/FI hydrogels. (D) Laser scanning confocal images of DRG spheres (green, $NF200^{+}$) and SCs (red, $S100^{+}$) cultured for 7 days on different hydrogels. (E) Neurite myelination after DRG cultivation for 30 days on different hydrogels. Cell nuclei were stained by DAPI in (D) and (E). (F) Statistical analysis of neurite length (a), number of SCs migrating away from DRG spheres as a function of migration distance (b) and the percentage of axon-attached SCs (c). DRG spheres were cultured for 7 days on different hydrogels. (G) Relative ERK2, AKT1 and MBP gene expressions on different hydrogels after culturing of DRG neurons for 30 days. *p < 0.05, **p < 0.01, and ***p < 0.001.

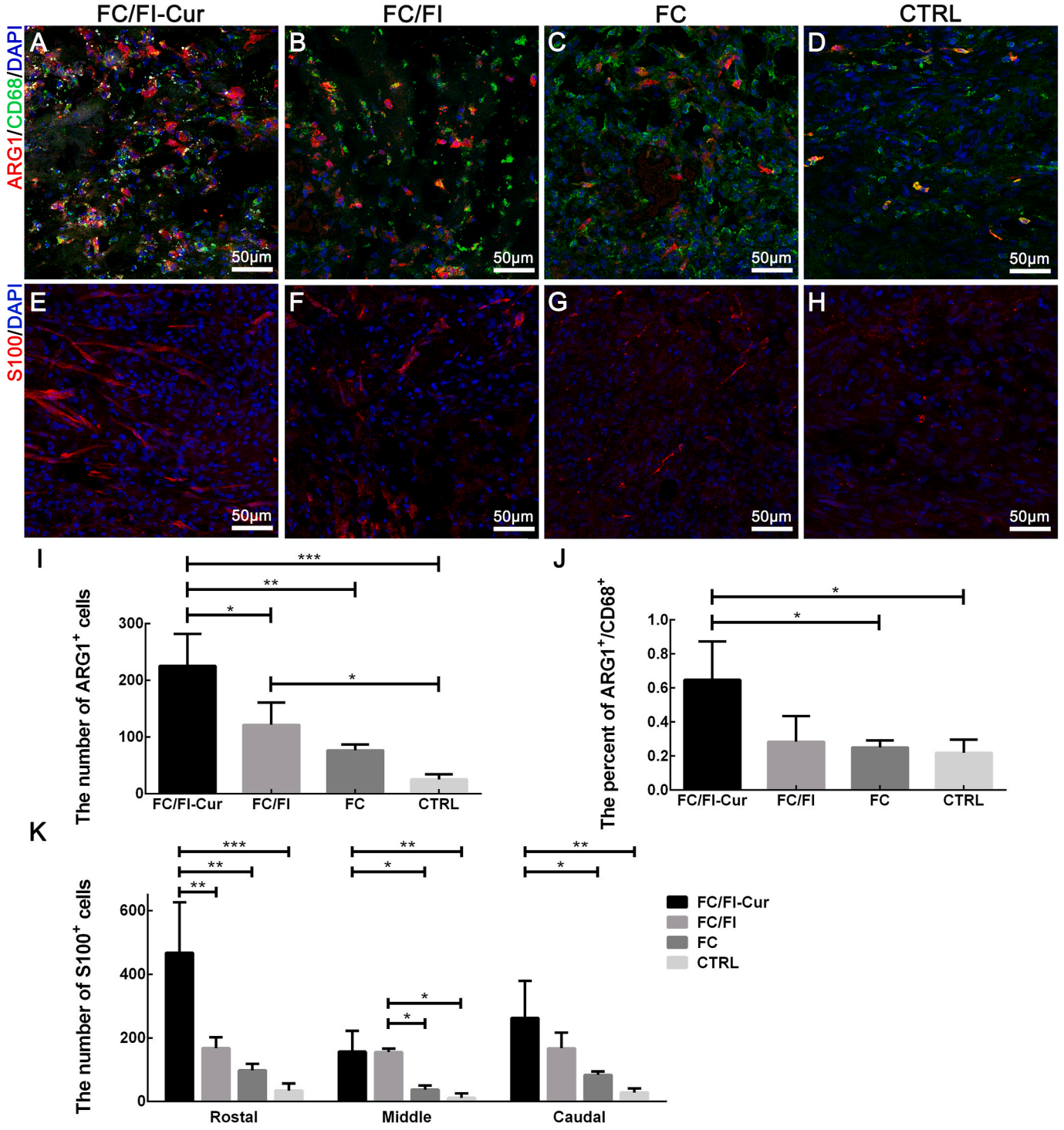

Fig. 7. Infiltration of macrophages/microglia cells and SCs in lesion sites 2 weeks after SCI. (A–D) were $CD68^{+}$ cells (green) and $ARG1^{+}$ cells (red) of different groups. (E–H) were SCs ($S100^{+}$, red) of different groups. Cell nuclei were stained by DAPI in (A–H). These images were from the sites labeled with "*" in Fig. S3. Quantitative analyses number of $ARG1^{+}$ (I), percent of $ARG1^{+}/CD68^{+}$ cells and number of $S100^{+}$ cells (K) in the lesion sites were presented. *P < 0.05, **P < 0.01, ***P < 0.001. (n = 6).

significantly more ARG1$^+$ cells infiltrating within the FC/FI-Cur hydrogel. Moreover, FC/FI-Cur hydrogel showed the highest percent of ARG1$^+$/CD68$^+$, significantly higher than the other three groups. These results suggested that FC/FI-Cur hydrogel could effectively regulate inflammatory cell phenotypes, which would potentially improve the microenvironment. Such inflammatory improvement was probably attributed to the well-known anti-oxidant and anti-inflammatory pharmacological activities of Cur [19].

SC infiltration within the lesion sites was also investigated 2 weeks after SCI. Numerous S100$^+$ SCs of bipolar spindle shape were found to invade into the FC/FI-Cur hydrogel from the nerve roots between the dura and hydrogel, whereas SCs were seldom observed in the lesion site of the CTRL group (Fig. S3 and Fig. 7). SC infiltration in the FC and FC/FI hydrogels was also observed, and the quantities of SCs in these two hydrogels were significantly lower as compared to that in FC/FI-Cur hydrogel (Fig. 7K). More SCs infiltration in FC/FI-Cur hydrogel was mainly attributed to the promotion of SC migration by Cur as shown in the cell studies above. The improved microenvironment in the lesion site due to the anti-oxidant and anti-inflammatory properties of Cur might also be responsible for SC infiltration.

Myelin regeneration or remyelination of spared and regenerating axons after SCI has garnered significant attention due to its great importance in signal transmission and neural functions [40]. Remyelination determined by double immunochemical staining of myelin basic protein (MBP) and NF200 was clearly observed within the FC/FI-Cur graft in the lesion site (Fig. 8A). Images of high magnification and their Z-stack scanning showed the intimate contact between neural filaments and the myelin sheath (Fig. 8a). Images of transversal section depicted that MBP$^+$ myelin sheath exhibited complete "O" rings, encircling neurofilament-immunoreactive axons (Fig. 8B). Such observation confirmed the remyelination in the FC/FI-Cur graft. TEM was further employed to investigate the structure of the regenerating nerves. As shown in Fig. 8C, typical layered myelin sheets were clearly observed to surround the axoplasm, in which the neurofilaments and vesicles could be found. SCs were well identified by their characteristic 1:1 relationship associated with myelinated axons via intact well recognized basal laminae in addition to scattered SCs (* in Fig. 8C) [41]. Therefore, SCs recruited into the FC/FI-Cur graft were supposed to participate in the remyelination process. SC-based remyelination occurred in FC/FI graft but significantly fewer MBP$^+$ myelin sheaths were observed in FC graft with certain axons completely devoid of myelin (Fig. S4). Few neurites and a particularly evident loss of MBP were observed in the

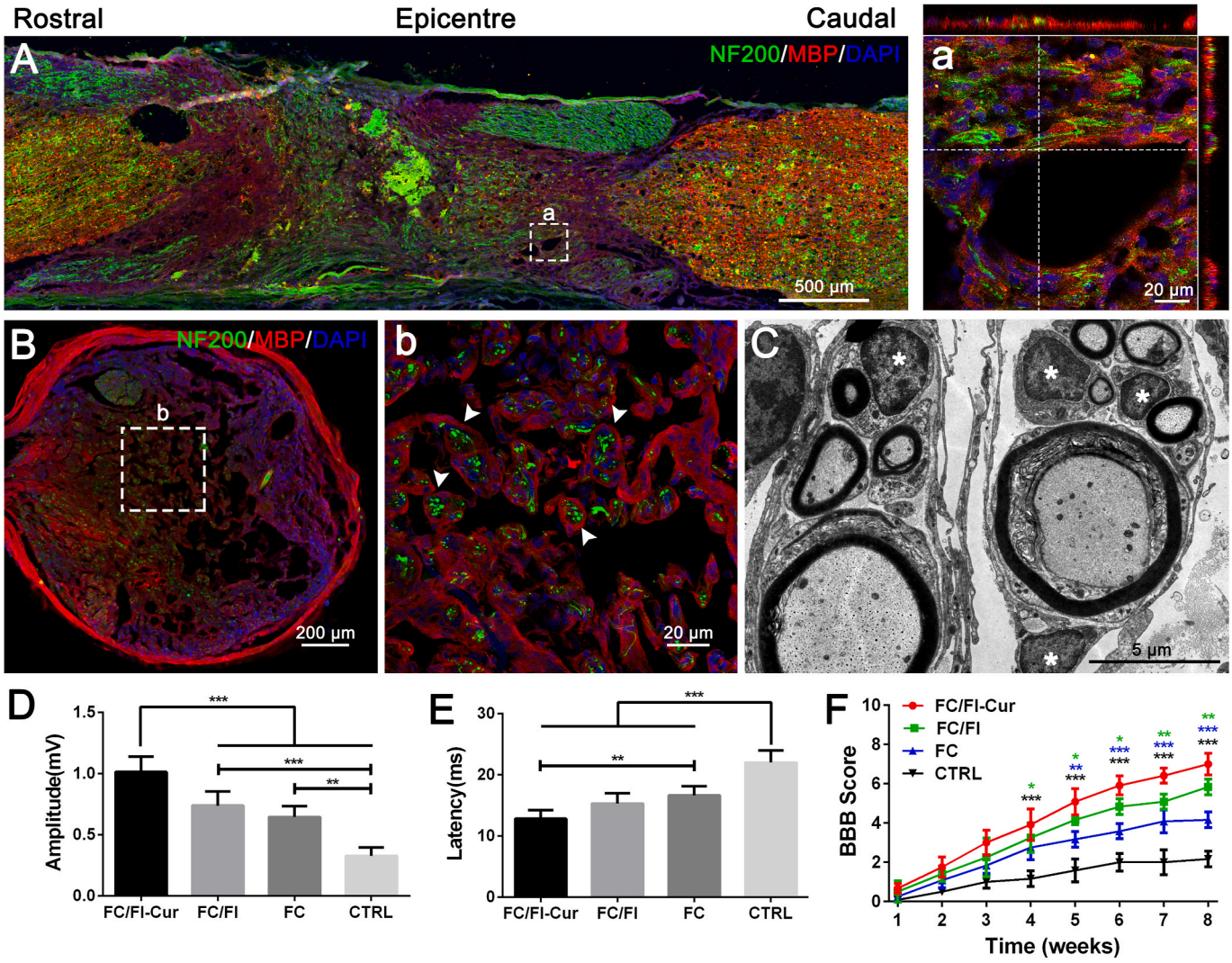

Fig. 8. Investigation on remyelination and functional recovery 2 months after implantation of FC/FI-Cur hydrogel following SCI. (A) Robust remyelination was detected in the graft. (a) Images of high magnification showed that nerve fibers were ensheathed by MBP positive myelin sheath. (B, b) Images of the transversal section in the lesion showed complete rings of myelin encircling axons. (C) Ultrastructural images of regenerated tissues in cross sections of the lesion were assessed by electron microscopy. (D) BBB open-field walking scale of rats with different treatments after SCI during the course of 8 weeks. (D) and (E) were the amplitude and latency of MEPs, respectively. *P < 0.05, **P < 0.01, ***P < 0.001. (n = 6).

lesion site of the CTRL group. Both thickness of myelin sheets and diameter of myelinated axons were found to increase in the sequence of CTRL, FC hydrogel, FC/FI hydrogel and FC/FI-Cur hydrogel, with significant differences existing in the pairwise comparisons. Spontaneous remyelination attributed to endogenous oligodendrogenesis would occur after SCI, but the low efficiency has remained a point of concern until now [6]. Transplantation of oligodendrocyte precursor cells [42] or neural progenitor cells for differentiating into oligodendrocytes in order to enhance myelination [43] are alternatives. However, cell transplantation suffers from limitations, such as cell sources, tumor risk and ethical issues. SCs are promising candidates facilitating myelination of axons. Although SCs are not observed in the central nervous system, they would migrate into the lesion site from the nerve roots following SCI, myelinating the regenerated or demyelinated axons in the injured spinal cord and then restoring conduction activity [7,8]. Our results demonstrated that endogenous remyelination after SCI was feasible and promising by the recruitment of endogenous SCs using bioactive hydrogels in combination with controlled release of Cur.

The main role of myelination is to restore conduction activity for signal transduction. MEPs, the reliable indicators of the capacity of electrical signal conduction widely used to detect SCI and the efficacy of interventions, were measured at 8 weeks after injury. The amplitude significantly decreased while the response latency increased in the order of CTRL, FC hydrogel, FC/FI hydrogel and FC/FI-Cur hydrogel (Fig. 8D and E). Since MEPs rely on conduction across the synapse between the upper and lower motor neurons [44], the improved electrophysiological properties suggested enhanced neural conduction through the injury site after treating with hydrogels, especially with the FC/FI-Cur hydrogel. As a result, motor function recovery was promoted as evaluated by BBB open-field walking score (Fig. 8F).

4. Conclusions

In this study, a hybrid hydrogel with injectable and self-healing properties was prepared from two Fmoc molecules, Fmoc-grafted chitosan (FC) and Fmoc peptide (FI). Abundant π-π stacking interactions of the fluorenyl rings acted as physically cross-linked points in the FC/FI hybrid hydrogel. Their dynamic reversibility endowed the hybrid hydrogel with good injectability and self-healability. Moreover, Cur encapsulated in the hybrid hydrogel had been released in a sustained pattern for the 7-day period. *In vitro* study showed that the FC/FI-Cur hybrid hydrogel accelerated neurite outgrowth of DRG neurons. SC migration away from DRG spheres was also enhanced, forming a tight association with the segregated axons and producing myelinated segments. The presented FC/FI-Cur hybrid hydrogel could well reassemble extracellular matrix locally at the lesion site of rat spinal cord, and further modulate local inflammatory reaction by regulating the phenotypes of infiltrated inflammatory cells. SCs were also recruited in the FC/FI-Cur graft to participate in the remyelination process of the regenerated nerves. These outcomes, taken together, proved the hydrogel's ability to facilitate functional recovery. Therefore, the current work advanced the development of a multifunctional hydrogel system in repairing SCI.

CRediT authorship contribution statement

Jinghua Luo: Conceptualization, Methodology, Writing – original draft. **Xueshuang Shi:** Conceptualization, Methodology, Writing – original draft. **Liming Li:** Formal analysis. **Zan Tan:** Investigation. **Feng Feng:** Visualization. **Jun Li:** Investigation, Validation. **Mao Pang:** Formal analysis. **Xiaoying Wang:** Methodology, Resources. **Liumin He:** Resources, Writing – review & editing, Supervision, Funding acquisition.

Declaration of competing interest

The authors declare that they have no known competing financial interests or personal relationships that could have appeared to influence the work reported in this paper.

Acknowledgements

This work was supported by the National Natural Science Foundation of China (31870964, 32071354), Natural Science Foundation of Guangdong Province (2018A030313858), Guangzhou People's Livelihood Science and Technology Tackling Project (201903010095), and the Fundamental Research Funds for the Central Universities to Sun Yat-sen University. The authors wish to thank Dr. Nuan Chen from Nanyang Technological University, Singapore for critical comments on the manuscript.

Appendix A. Supplementary data

Supplementary data to this article can be found online at https://doi.org/10.1016/j.bioactmat.2021.05.022.

References

[1] A. Ackery, C. Tator, A. Krassioukov, A global perspective on spinal cord injury epidemiology, J. Neurotrauma 21 (10) (2004) 1355–1370.
[2] C.S. Ahuja, S. Nori, L. Tetreault, J. Wilson, B. Kwon, J. Harrop, D. Choi, M. G. Fehlings, Traumatic spinal cord injury-repair and regeneration, Neurosurgery 80 (3S) (2017) S9–S22.
[3] P. Lu, Y. Wang, L. Graham, K. McHale, M. Gao, D. Wu, J. Brock, A. Blesch, E. S. Rosenzweig, L.A. Havton, B. Zheng, J.M. Conner, M. Marsala, M.H. Tuszynski, Long-distance growth and connectivity of neural stem cells after severe spinal cord injury, Cell 150 (6) (2012) 1264–1273.
[4] P. Assinck, G.J. Duncan, B.J. Hilton, J.R. Plemel, W. Tetzlaff, Cell transplantation therapy for spinal cord injury, Nat. Neurosci. 20 (5) (2017) 637–647.
[5] C.D. Thompson, J.C. Zurko, B.F. Hanna, D.J. Hellenbrand, A. Hanna, The therapeutic role of interleukin-10 after spinal cord injury, J. Neurotrauma 30 (15) (2013) 1311–1324.
[6] G.J. Duncan, S.B. Manesh, B.J. Hilton, P. Assinck, J.R. Plemel, W. Tetzlaff, The fate and function of oligodendrocyte progenitor cells after traumatic spinal cord injury, Glia 68 (2) (2020) 227–245.
[7] N. Nagoshi, S. Shibata, M. Hamanoue, Y. Mabuchi, Y. Matsuzaki, Y. Toyama, M. Nakamura, H. Okano, Schwann cell plasticity after spinal cord injury shown by neural crest lineage tracing, Glia 59 (5) (2011) 771–784.
[8] S. Casha, W.R. Yu, M.G. Fehlings, Oligodendroglial apoptosis occurs along degenerating axons and is associated with FAS and p75 expression following spinal cord injury in the rat, Neuroscience 103 (1) (2001) 203–218.
[9] H. Kanno, Y. Pressman, A. Moody, R. Berg, E.M. Muir, J.H. Rogers, H. Ozawa, E. Itoi, D.D. Pearse, M.B. Bunge, Combination of engineered Schwann cell grafts to secrete neurotrophin and chondroitinase promotes axonal regeneration and locomotion after spinal cord injury, J. Neurosci. 34 (5) (2014) 1838–1855.
[10] H. Liu, X. Xu, Y. Tu, K. Chen, L. Song, J. Zhai, S. Chen, L. Rong, L. Zhou, W. Wu, K. F. So, S. Ramakrishna, L. He, Engineering microenvironment for endogenous neural regeneration after spinal cord injury by reassembling extracellular matrix, ACS Appl. Mater. Interfaces 12 (15) (2020) 17207–17219.
[11] R.C. Assuncao-Silva, E.D. Gomes, N. Sousa, N.A. Silva, A.J. Salgado, Hydrogels and cell based therapies in spinal cord injury regeneration, Stem Cell. Int. 2015 (2015), 948040.
[12] Y. Tu, N. Chen, C. Li, H. Liu, R. Zhu, S. Chen, Q. Xiao, J. Liu, S. Ramakrishna, L. He, Advances in injectable self-healing biomedical hydrogels, Acta Biomater. 90 (2019) 1–20.
[13] Z. Qiao, X. Lv, S. He, S. Bai, X. Liu, L. Hou, J. He, D. Tong, R. Ruan, J. Zhang, J. Ding, H. Yang, A mussel-inspired supramolecular hydrogel with robust tissue anchor for rapid hemostasis of arterial and visceral bleedings, Bioact. Mater. 6 (9) (2021) 2829–2840.
[14] Y. Luo, F. Xue, K. Liu, B. Li, C. Fu, J. Ding, Physical and biological engineering of polymer scaffolds to potentiate repair of spinal cord injury, Mater. Des. 201 (2021), 109484.
[15] Q. Zhang, B. Shi, J. Ding, L. Yan, J.P. Thawani, C. Fu, X. Chen, Polymer scaffolds facilitate spinal cord injury repair, Acta Biomater. 88 (2019) 57–77.
[16] Y. Xu, Y. Li, Q. Chen, L. Fu, L. Tao, Y. Wei, Injectable and self-healing chitosan hydrogel based on imine bonds: design and therapeutic applications, Int. J. Mol. Sci. 19 (8) (2018).
[17] T.C. Tseng, L. Tao, F.Y. Hsieh, Y. Wei, I.M. Chiu, S.H. Hsu, An injectable, self-healing hydrogel to repair the central nervous system, Adv. Mater. 27 (23) (2015) 3518–3524.
[18] Y. Liu, Y.H. Hsu, A.P. Huang, S.H. Hsu, Semi-interpenetrating polymer network of hyaluronan and chitosan self-healing hydrogels for central nervous system repair, ACS Appl. Mater. Interfaces 12 (36) (2020) 40108–40120.
[19] S.C. Gautam, X. Gao, S. Dulchavsky, Immunomodulation by curcumin, Adv. Exp. Med. Biol. 595 (2007) 321–341.
[20] R. Sanivarapu, V. Vallabhaneni, V. Verma, The potential of curcumin in treatment of spinal cord injury, Neurol. Res. Int. 2016 (2016), 9468193.

[21] W. Li, S. Yao, H. Li, Z. Meng, X. Sun, Curcumin promotes functional recovery and inhibits neuronal apoptosis after spinal cord injury through the modulation of autophagy, J. Spinal Cord Med. 44 (1) (2021) 37–45.
[22] G.M. Liu, K. Xu, J. Li, Y.G. Luo, Curcumin upregulates S100 expression and improves regeneration of the sciatic nerve following its complete amputation in mice, Neural Regen. Res. 11 (8) (2016) 1304–1311.
[23] Z. Zhao, X. Li, Q. Li, Curcumin accelerates the repair of sciatic nerve injury in rats through reducing Schwann cells apoptosis and promoting myelinization, Biomed. Pharmacother. 92 (2017) 1103–1110.
[24] Y. Liu, D. Li, J. Ding, X. Chen, Controlled synthesis of polypeptides, Chin. Chem. Lett. 31 (12) (2020) 3001–3014.
[25] K. Tao, A. Levin, L. Adler-Abramovich, E. Gazit, Fmoc-modified amino acids and short peptides: simple bio-inspired building blocks for the fabrication of functional materials, Chem. Soc. Rev. 45 (14) (2016) 3935–3953.
[26] L. He, S. Liao, D. Quan, M. Ngiam, C.K. Chan, S. Ramakrishna, J. Lu, The influence of laminin-derived peptides conjugated to Lys-capped PLLA on neonatal mouse cerebellum C17.2 stem cells, Biomaterials 30 (8) (2009) 1578–1586.
[27] D. Wu, S. Zhang, Y. Zhao, N. Ao, S. Ramakrishna, L. He, The effects of motif net charge and amphiphilicity on the self-assembly of functionally designer RADA16-I peptides, Biomed. Mater. 13 (3) (2018), 035011.
[28] Y. Sun, Y. Zhang, L. Tian, Y. Zhao, D. Wu, W. Xue, S. Ramakrishna, W. Wu, L. He, Self-assembly behaviors of molecular designer functional RADA16-I peptides: influence of motifs, pH, and assembly time, Biomed. Mater. 12 (1) (2016), 015007.
[29] C. Diaferia, G. Morelli, A. Accardo, Fmoc-diphenylalanine as a suitable building block for the preparation of hybrid materials and their potential applications, J. Mater. Chem. B 7 (34) (2019) 5142–5155.
[30] J.B. Matson, S.I. Stupp, Self-assembling peptide scaffolds for regenerative medicine, Chem. Commun. 48 (1) (2012) 26–33.
[31] M.M. Denn, J.F. Morris, D. Bonn, Shear thickening in concentrated suspensions of smooth spheres in Newtonian suspending fluids, Soft Matter 14 (2) (2018) 170–184.
[32] L. Li, B. Yan, J. Yang, W. Huang, L. Chen, H. Zeng, Injectable self-healing hydrogel with antimicrobial and antifouling properties, ACS Appl. Mater. Interfaces 9 (11) (2017) 9221–9225.
[33] C. Tang, R.V. Ulijn, A. Saiani, Effect of glycine substitution on Fmoc-diphenylalanine self-assembly and gelation properties, Langmuir 27 (23) (2011) 14438–14449.
[34] C. Tang, R.V. Ulijn, A. Saiani, Self-assembly and gelation properties of glycine/leucine Fmoc-dipeptides, Eur. Phys. J. E Soft Matter 36 (10) (2013) 111.
[35] J.W. Sadownik, J. Leckie, R.V. Ulijn, Micelle to fibre biocatalytic supramolecular transformation of an aromatic peptide amphiphile, Chem. Commun. 47 (2) (2011) 728–730.
[36] M. Zhou, A.M. Smith, A.K. Das, N.W. Hodson, R.F. Collins, R.V. Ulijn, J.E. Gough, Self-assembled peptide-based hydrogels as scaffolds for anchorage-dependent cells, Biomaterials 30 (13) (2009) 2523–2530.
[37] A.R. Deshmukh, H. Aloui, C. Khomlaem, A. Negi, J.H. Yun, H.S. Kim, B.S. Kim, Biodegradable films based on chitosan and defatted Chlorella biomass: functional and physical characterization, Food Chem. 337 (2021), 127777.
[38] C. Wang, M. Wang, K. Xia, J. Wang, F. Cheng, K. Shi, L. Ying, C. Yu, H. Xu, S. Xiao, C. Liang, F. Li, B. Lei, Q. Chen, A bioactive injectable self-healing anti-inflammatory hydrogel with ultralong extracellular vesicles release synergistically enhances motor functional recovery of spinal cord injury, Bioact. Mater. 6 (8) (2021) 2523–2534.
[39] A. Ahmed, A.A. Patil, D.K. Agrawal, Immunobiology of spinal cord injuries and potential therapeutic approaches, Mol. Cell. Biochem. 441 (1–2) (2018) 181–189.
[40] N. Pukos, M.T. Goodus, F.R. Sahinkaya, D.M. McTigue, Myelin status and oligodendrocyte lineage cells over time after spinal cord injury: what do we know and what still needs to be unwrapped? Glia 67 (11) (2019) 2178–2202.
[41] R.E. Ward, W. Huang, M. Kostusiak, P.N. Pallier, A.T. Michael-Titus, J.V. Priestley, A characterization of white matter pathology following spinal cord compression injury in the rat, Neuroscience 260 (2014) 227–239.
[42] N. Egawa, K.K. Chung, R. Takahashi, E.H. Lo, H. Inoue, K. Arai, Brief review: can modulating DNA methylation state help the clinical application of oligodendrocyte precursor cells as a source of stem cell therapy? Brain Res. 1723 (2019), 146386.
[43] S.R. Sankavaram, R. Hakim, R. Covacu, A. Frostell, S. Neumann, M. Svensson, L. Brundin, Adult neural progenitor cells transplanted into spinal cord injury differentiate into oligodendrocytes, enhance myelination, and contribute to recovery, Stem Cell Rep. 12 (5) (2019) 950–966.
[44] W.S. Jellish, Motor-evoked potentials are an important determinant of spinal cord ischemic injury during aortic arch surgery. But can they Be used exclusively? J. Cardiothorac. Vasc. Anesth. 33 (7) (2019) 1843–1844.